Time meets space – brain dynamics drive spatial topography

Mehrshad Golesorkhi[1,2], Shankar Tumati[2], Javier Gomez-Pilar[3,4], Emmanuel. A. Stamatakis[5,6], Georg. Northoff[2,7,8]*

1. School of Electrical Engineering and Computer Science, University of Ottawa, Ottawa, Canada.
2. Mind, Brain Imaging and Neuroethics Research Unit, Institute of Mental Health, Royal Ottawa Mental Health Centre and University of Ottawa, Ottawa, Canada.
3. Biomedical Engineering Group, University of Valladolid, Paseo de Belén, 15, 47011 Valladolid, Spain.
4. Centro de Investigación Biomédica en Red en Bioingeniería, Biomateriales y Nanomedicina, (CIBER-BBN), Spain.
5. Division of Anaesthesia, School of Clinical Medicine, University of Cambridge, Cambridgeshire, England, United Kingdom.
6. Department of Clinical Neurosciences, School of Clinical Medicine, University of Cambridge, Cambridgeshire, England, United Kingdom.
7. Centre for Cognition and Brain Disorders, Hangzhou Normal University, Hangzhou, China.
8. Mental Health Centre, Zhejiang University School of Medicine, Hangzhou, Zhejiang, China.

Abstract

The brain exhibits both spatial and temporal hierarchy with their relationship remaining an open question. We address this issue by investigating the brain's spatial hierarchy with complexity, i.e., Lempel-Zev Complexity (LZC) and temporal dynamics, i.e., median frequency (MF) in rest/task fMRI (including replication data). Our results are: (I) topographical differences in rest between higher-order networks (lower LZC and MF) and lower-order networks (higher LZC and MF); (II) task-specific increases and task-unspecific decreases in LZC and MF; (III) non-linear topographical relationship with low MF mediating higher LZC rest-task changes as confirmed in various simulations. Together, we demonstrate convergence of spatial (LZC) and temporal (MF) hierarchies in a non-linear topographical way along the lines of higher-order/slow frequency and lower-order/fast frequency networks.

Introduction

There is a converging evidence for spatial topography in the human cerebral cortex with lower-order sensory networks and higher-order association network at opposite ends of the hierarchy [1–4]. The spatial topography is already present in rest and carried over to task states [5,6]. At the same time, there is increasing evidence for temporal hierarchy in the cortex with different regions exhibiting different temporal dynamics like slow and fast frequency power [7,8,17–22,9–16].

How such temporal hierarchy is related to and modulates the spatial topography including how their convergence shapes rest and task states remains yet unclear. Using fMRI and simulation, we here show that the spatial hierarchy of lower- and higher-order networks in terms of their levels of complexity is related to their temporal dynamics, i.e., slower and faster frequency power, in a non-linear topographical way. That provides a novel understanding how the brain's spatial and temporal dimensions converge by shaping cortical activity distribution in a non-linear topographical way during rest and the transition from rest to task states.

The brain's spontaneous activity exhibits fluctuations in different frequency ranges. These include faster frequencies from 1Hz to 240Hz [23] as well as slower ones like the slow cortical potentials (0.1hz to 1Hz) which all can be measured using EEG or MEG [24–28]. These different frequencies have been associated with diverse functions including perception, attention, working memory, self, motivation, and consciousness (and various others) [23,29]. In contrast, the exact role of the more powerful slower frequencies (slow: 0.1 to 1Hz, infraslow: < 0.1Hz) for the brain's various functions like perception and cognition remains poorly understood (see [24,30]). There is strong evidence that infraslow frequencies (ISF) strongly shape the brain's spatial topography as reflected in the various resting state networks [1–4].

Various fMRI studies demonstrate evidence of topographical organization with lower-order networks, i.e., sensory networks, and higher-order networks, i.e., default-mode network, executive network, and others, standing at opposite ends of the spatial hierarchy [1–6,31]. That is further supported by showing that lower-order networks exhibit stimulus-dependence and content homogeneity while activity in higher-order networks remains rather stimulus-independent and content heterogenous [1,2]. Are lower- and higher-order networks including their distinct positions within the spatial hierarchy related to distinct temporal features? This is the main focus of our study.

Parallel to the spatial topography, several investigators observed temporal hierarchy with different regions exhibiting different durations in their temporal features during various task states [7,8,17–19,32,33,9–16]. Whether such temporal hierarchy is intrinsic and thus already present during the resting state in its infraslow frequencies remains not yet fully clear. In that case, one would expect convergence of spatial and temporal hierarchies: the temporal features of lower- and higher-order networks, as based on their spatial topography, should differ in rest which should then also mediate their transition from rest to task states in differential ways. The main contribution of our study is to provide this missing link, that is, the connection of spatial and temporal dimensions in the brain's lower-higher-order network topographical hierarchy.

Main aim - complexity (LZC) and power spectral density (MF)

The main aim of our study was to investigate the convergence of spatial and temporal topographies including how that shapes rest and task states. For that purpose, we used the Human Connectome Project (HCP) 7 Tesla fMRI datasets (and the HCP 3T for replication) applying novel measures like Lempel-Ziv complexity (LZC) and median frequency (MF) during different states, i.e., rest and two different task states with two completely different complexity and temporal structure (i.e., movie and retinotopy) (see below).

LZC measures the number of distinct patterns in a binary sequence i.e., the regularity or repetitiveness of a signal [34,35], which reflects the amount of information (number of bits) required to reconstruct a signal [34]. Recently, LZC has been applied in fMRI [36–39] as well as in other imaging modalities including MEG [40–43] and

EEG (Abasólo et al., 2007; Abásolo et al., 2006; Bachmann et al., 2018; Ibáñez-Molina et al., 2018; Mateos et al., 2018, Schartner et al. 2015, 2017, Andrillon et al., 2016; Ferenets et al., 2007) (and also on the cellular level., i.e., spike train (Szczepański et al., 2003, Dasilva et al. 2020, in revision)) during both rest and task states. This makes complexity, i.e., LZC an excellent candidate to characterize the complexity of the ISF's neural processing and their spatial topography during both rest and task states.

The LZC was complemented by a measure of temporal dynamics, that is, median frequency (MF) that measures the distribution of the power spectral density across a specific frequency range like the ISF [50–54] (see also [8] for a related measure, the mean frequency). Combining LZC with MF allowed us to directly link spatial topography of different complexities (LZC) in different regions with the concurrent determination of their temporal dynamics, i.e., their power spectral density (MF). (see Fig. 1 for general overview).

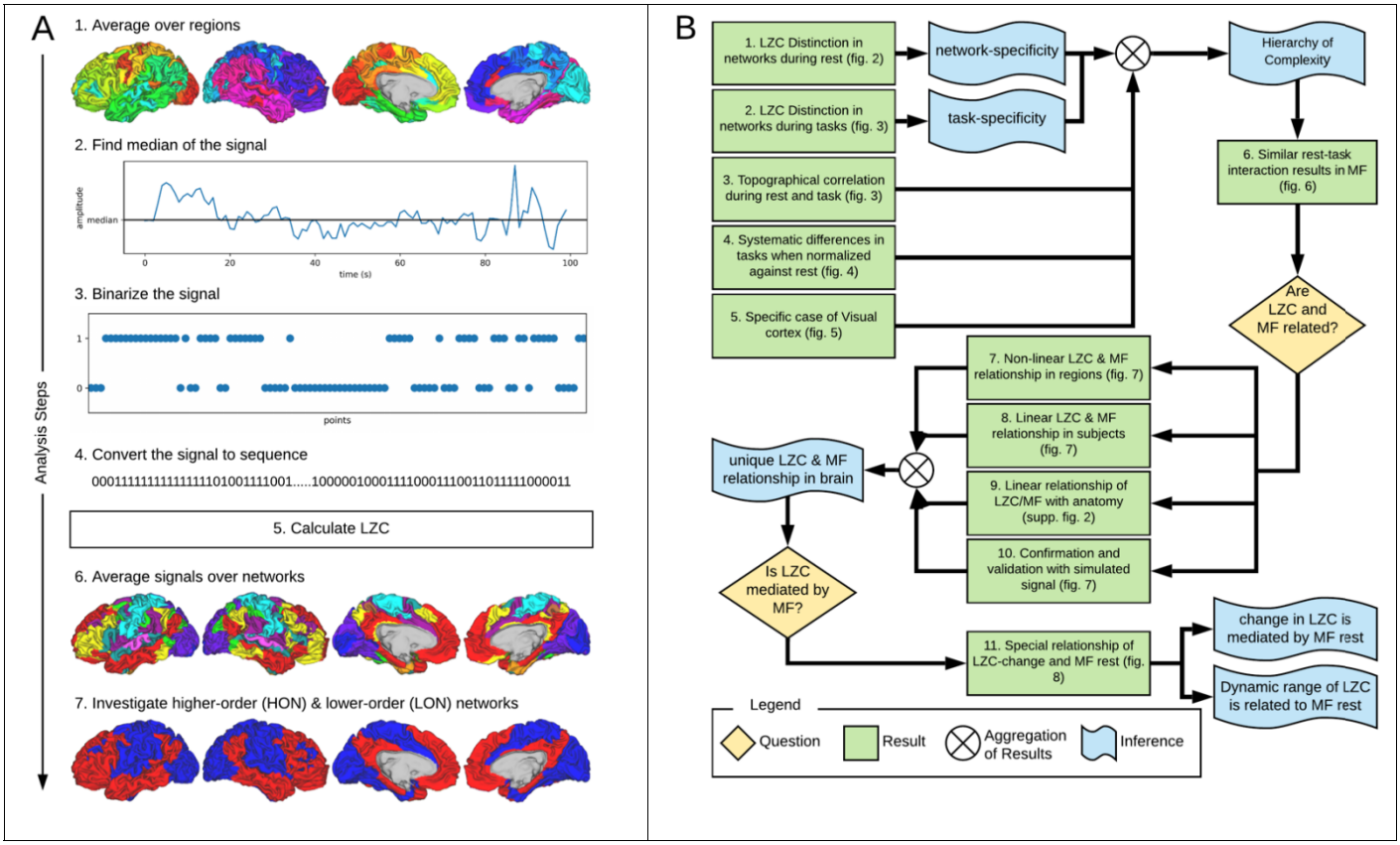

Fig. 1. Schema of the paper. (A) *The major steps involved in the LZC computation over the brain. First, signals were averaged to form 712 regions defined in the template provided by [60]. Then, each signal was binarized by considering its own median. The binary signal was converted to a 0-1 sequence and fed to the LZC algorithm. Finally, then LZC values were average over the 12 networks and also LON, HON division.* ***(B)*** *The sequence of results and findings with their corresponding figure.*

Specific aims and hypotheses

The first specific aim was to investigate LZC of ISF in rest and task states. Based on the well-known spatial differentiation of lower- and higher-order regions/networks [1–3,12,14,16,32,33,55] and LZC findings [36,38,42,43,56], we hypothesized different LZC values in these regions/networks, i.e., network-specific LZC, during both rest and task states. As most likely related to their continuous exposure to external highly irregular stimuli [1,2,12,32,33], lower-order regions like sensory networks and multimodal sensory regions may show higher LZC, i.e., more complexity and less regularity, than higher-order regions, i.e., default-mode network (DMN), frontoparietal network (FPN), language network, and dorsal attention network [1,32,33].

The second specific aim was to investigate regional temporal dynamics by using median frequency (MF) of ISF in rest and task states. Recent studies demonstrated that lower- and higher-order regions exhibit different intrinsic neural time scales with short and long durations in their temporal receptive windows during task states [7,8,17–19,32,33,9–16]. Based on these findings and the fact that the duration of intrinsic neural time scale may be related to the length of cycle durations [57] as reflecting the frequency range [7,8], we hypothesized that lower-order networks would exhibit higher MF, i.e., stronger power in faster ISF frequency ranges with shorter cycle duration. While we assumed that higher-order ones would show lower MF with stronger power in slower ISF frequency ranges, i.e., longer cycle durations, in both rest and task states.

The third specific aim consisted in directly linking spatial, i.e., LZC, and temporal, i.e., MF dimensions including their respective topographies. For that purpose, we conducted correlation and regression models as well as simulation. Given the scale-free driven discrepancy in power of slower (strong power) and faster (weaker power) ISF frequency ranges [7,13,58,59], we assumed non-linear topographical relationship of LZC and MF across lower- (weaker faster power) and higher- (stronger slower power) order network regions during both rest and rest-task transition.

The rationale here is the following: the slower the frequency (low MF) and the longer and the more regular its cycle durations [23,24,30], the lower the LZC should be as it measures the complexity of the signal through its regularity [7,24,30,57]. We therefore hypothesized that the degrees of LZC in rest and rest-task change are related to the level of MF, i.e., low or high. Due to the fact that the slower ISF frequency range (in the higher-order network regions) display disproportionately stronger power than faster ISF frequency ranges (in the lower-order networks region), we hypothesized non-linear topographical relationship of MF and LZC during both rest and transition from rest to task states. Specifically, we hypothesized that regions with low MF in rest may allow for larger LZC rest-task changes than regions exhibiting fast MF in rest.

Results

The topography of LZC during the resting state

Our first question was to investigate the spatial distribution of LZC in the resting state (see below for simulation on the validity of LZC measurement in fMRI). Observing the regional distribution of LZC values (Fig. 2A) suggested a specific spatial pattern of LZC during rest along the lines of lower- (LON) and higher-order (HON) networks. Visual1, visual2, auditory, somatomotor, posterior multimodal, ventral multimodal and orbitoaffective networks were categorized as lower-order and language, dorsal attention, cingulo opercular, frontoparietal and default-mode as higher-order networks (Here, it is important to mention that the LON is lower-order with respect to HON. We also did another more conservative division (LIH division) in which visuals, auditory and somatomotor were put in the lower-order category and cingulo opercular, frontoparietal and default-mode in the higher-order category. This division also replicated our results in Supp. Fig. 1).

In order to statistically test the LZC difference along the lines of LON and HON division, after preprocessing and high-pass filtering ($f > 0.01$, details are provided in the method section), the regions were divided and averaged into LON and HON based on the template provided by [60]. Paired student's t-test between LON and HON across subjects showed that LZC is significantly higher ($T = 42.20$, $p < 0.001$) in LON compared to HON (Fig. 2B). We then further investigated the topographical distribution of LZC over all of the 12 networks (Fig. 2C). Performing one-way ANOVA over the 12 networks across subjects revealed significant differences between them ($F(11, 1740) = 882.3$, $p < 0.001$). Together, these results show clear topographical differences in the spatial distribution of LZC with lower-order networks showing higher LZC than higher-order-networks (These results were also replicated in our 3T replication dataset in Supp. Fig. 7).

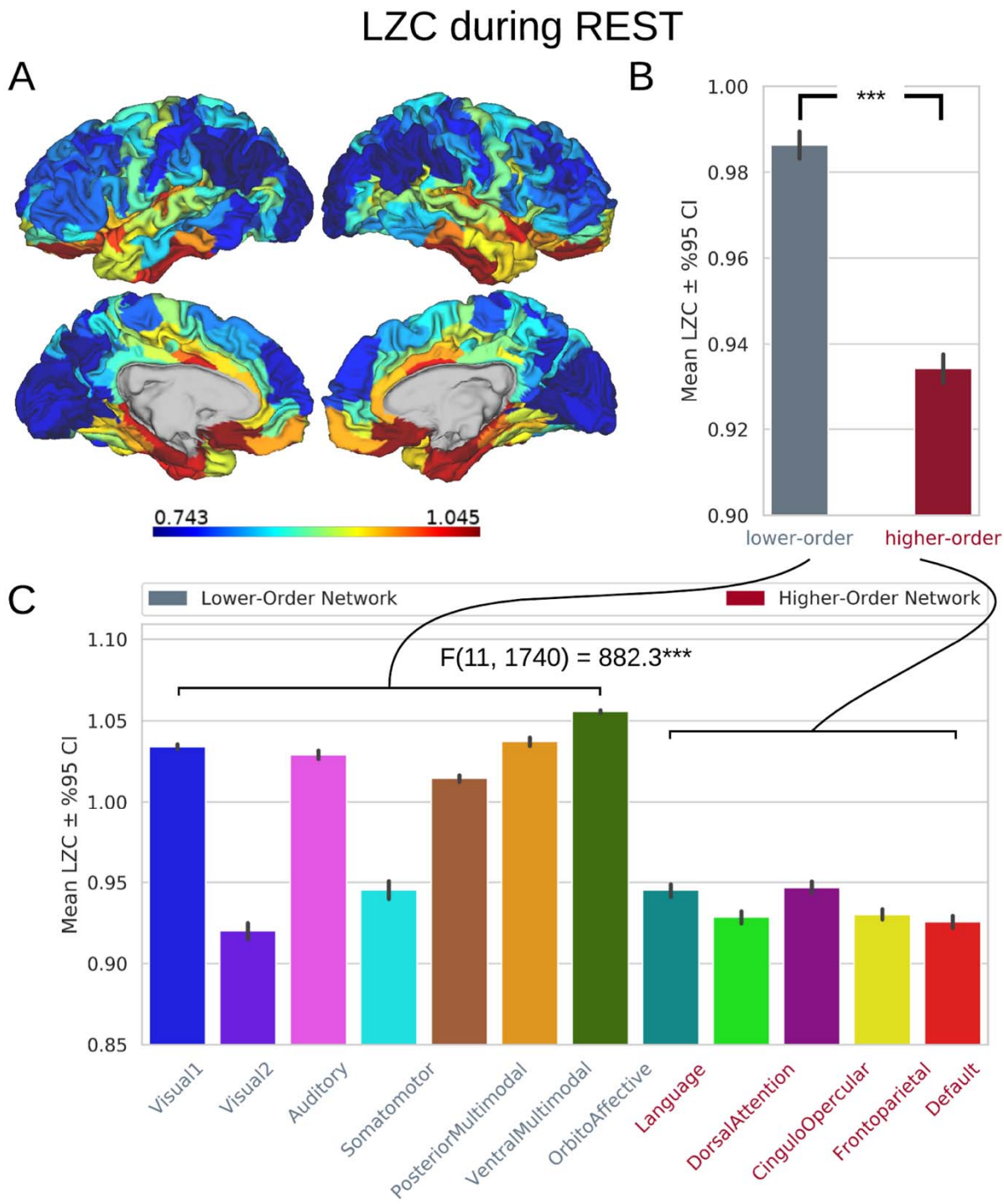

Fig. 2. LZC during the resting state. *All bars are the averaged LZC ± %95 confidence interval over subjects.* ***(A)*** *Spatial distribution of LZC during REST condition.* ***(B)*** *LZC during rest for lower- and higher-order networks. The paired student's t-test between LON and HON is significant with T = 42.20 at* $\alpha = 0.001$. ***(C)*** *LZC during rest for the 12 networks. One-way ANOVA showed a significant difference among the networks with F(11, 1740) = 882.3 at* $\alpha = 0.001$

The topography of LZC during task states

Spatial distribution of LZC was investigated during the two tasks of movie-watching (MOVIE) and retinotopy (RET) in three different ways: analysis of absolute values, spatial correlations, and analysis of percentage changes, i.e., rest-task difference. The two tasks have different complexity and temporal structure;

one containing rich stimuli of movie clips viewed in long intervals and one containing very simple retinotopic stimuli viewed in short intervals.

First, similar to our resting state analysis, LZC values were calculated for LON and HON (Fig. 3A) and their difference was statistically tested across subjects which revealed that in both tasks, similar to the resting state, LZC in LON is significantly (MOVIE: $T = 36.80$, RET: $T = 23.73$, $p < 0.001$) higher than in HON (Also replicated with LIH division). Moreover, dividing the LZC values into the 12 networks (Fig. 3B) and conducting one-way ANOVA on them also showed significant differences between the networks in both tasks (MOVIE: $F(11, 1740) = 2282.8$, RET: $F(11, 1728) = 1119.0$, $p < 0.001$).

The differences between networks in the tasks were analogous to the previous resting state results, suggesting that the topography of LZC during task states was similar to the resting state. To test this hypothesis, we, in a second analysis, calculated the spatial correlation among the three conditions of REST, MOVIE and RET (Fig. 3C). For each pair of conditions, LZC values were first averaged across subjects yielding a pair of LZC maps, then the two maps were correlated over regions yielding a single correlation. The result showed high correlation coefficients (Fig. 3C) in all combinations of conditions. These data, further support the assumption that the resting state LZC topography is also preserved during the two tasks.

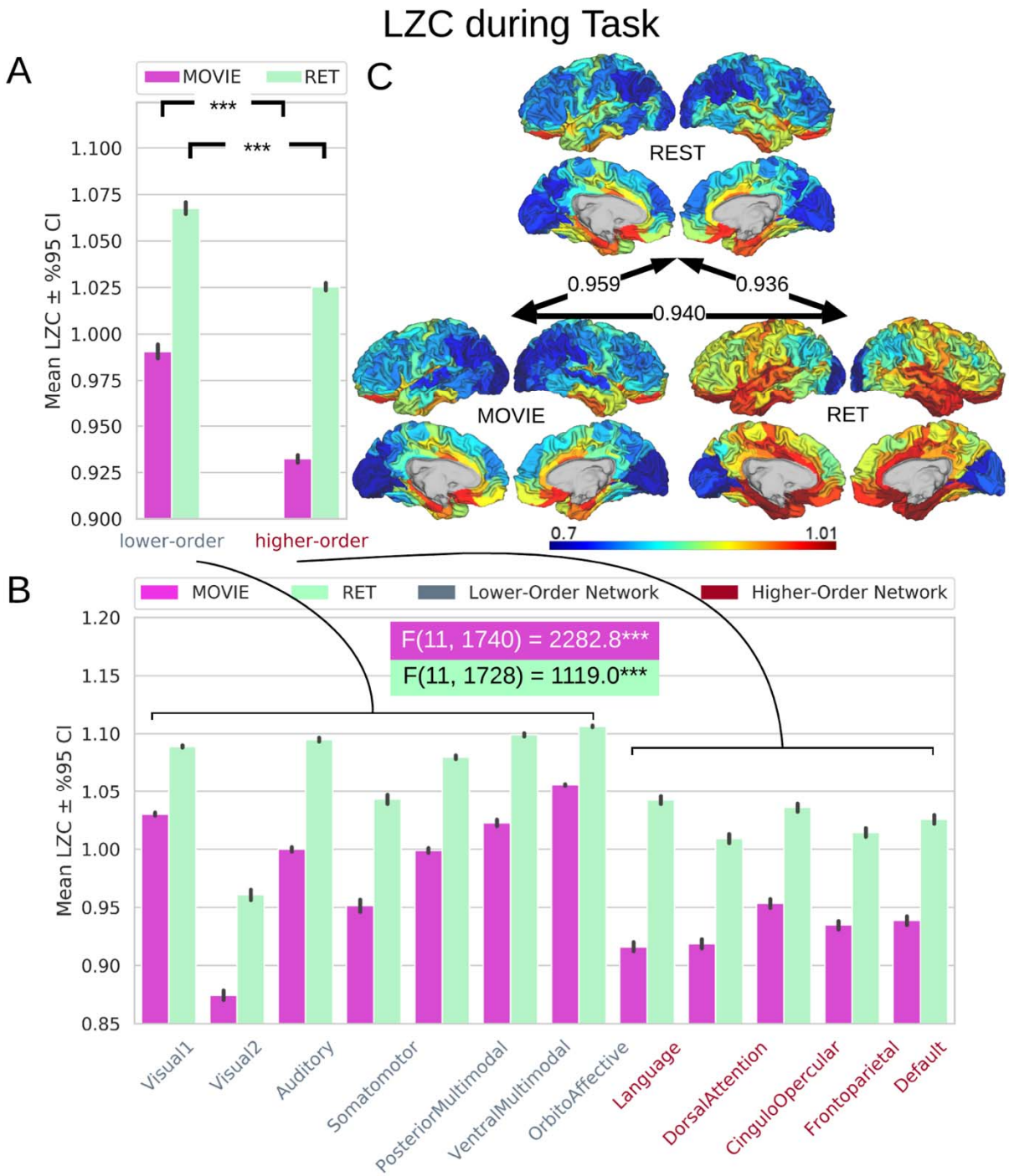

Fig. 3. LZC during the task states. *All bars are the averaged LZC ± 95% confidence interval over subjects.* ***(A)*** *LZC during MOVIE and RET for lower- and higher-order networks. The paired student's t-test between LON and HON is significant with T = 36.80 for MOVIE and T = 23.73 for RET at* $\alpha = 0.001$. ***(B)*** *LZC during the two task conditions for the 12 networks. One-way ANOVA showed a significant difference among the networks with F(11, 1740) = 2282 for MOVIE and F(11, 1728) = 1119 for RET at* $\alpha = 0.001$. ***(C)*** *Spatial distribution of LZC during REST, MOVIE and RET conditions alongside their 2-by-2 spatial correlation.*

Despite the fact that resting state LZC topography was carried over from rest to task, we nevertheless observed increases and decreases in LZC during the two task states. Therefore, in a third step, we calculated the percent of change of each region's LZC in task from its corresponding value during rest, thus normalizing LZC-change (LZCc) relative to resting state, i.e., rest-task difference. In other words, LZCc represents the LZC change from rest to task. Although LZCc was statistically different between LON and HON (MOVIE: T

= 19.54, RET: T = 24.97, $p < 0.001$), and over the 12 networks (MOVIE: $F(11, 1728) = 182.04$, RET: $F(11, 1728) = 329.8$, $p < 0.001$), it presented distinctive results for the two tasks (Fig. 4). In the MOVIE, positive LZCc values (increase in LZC from REST to MOVIE) were observed in visual, auditory, and language networks. In contrast, LZC values were prominently decreased from REST to RET (negative LZCc) in all networks.

The increase in LZC of visual, auditory and language networks from REST to MOVIE suggest a task-specific increase in complexity of task-related networks (also see [61] for a task-specific increase of entropy, a related measure to complexity, in motor cortex during a motor task). To further test for task-specific LZC changes, we specifically focused on the visual cortex during the RET task, a specifically and exclusively visual task. Previous literature has shown that retinotopic stimuli engage specific regions of the visual networks [62]. Thus, in order to specify our RET LZCc results, we decided to break the visual network into its different regions based on the template provided by Wang et al. (Supp. Fig. 2A). LZC values during the three conditions (Supp. Fig. 2B), and also the LZCc values (Supp. Fig. 2C) showed a prominent increase of LZC (positive LZCc, similar to the MOVIE) in primary visual areas such as V1, V2, and V3 from REST to RET. Hence, our results show an increase in LZC (positive LZCc) from REST to RET in those regions that are assumed to be involved in the task.

Taken together, LZC topography during rest along the lines of lower- and higher-order networks is largely preserved during and thus carried over to the different task states. Additionally, one can nevertheless observe task-related changes in LZC with task-specific increases in LZC.

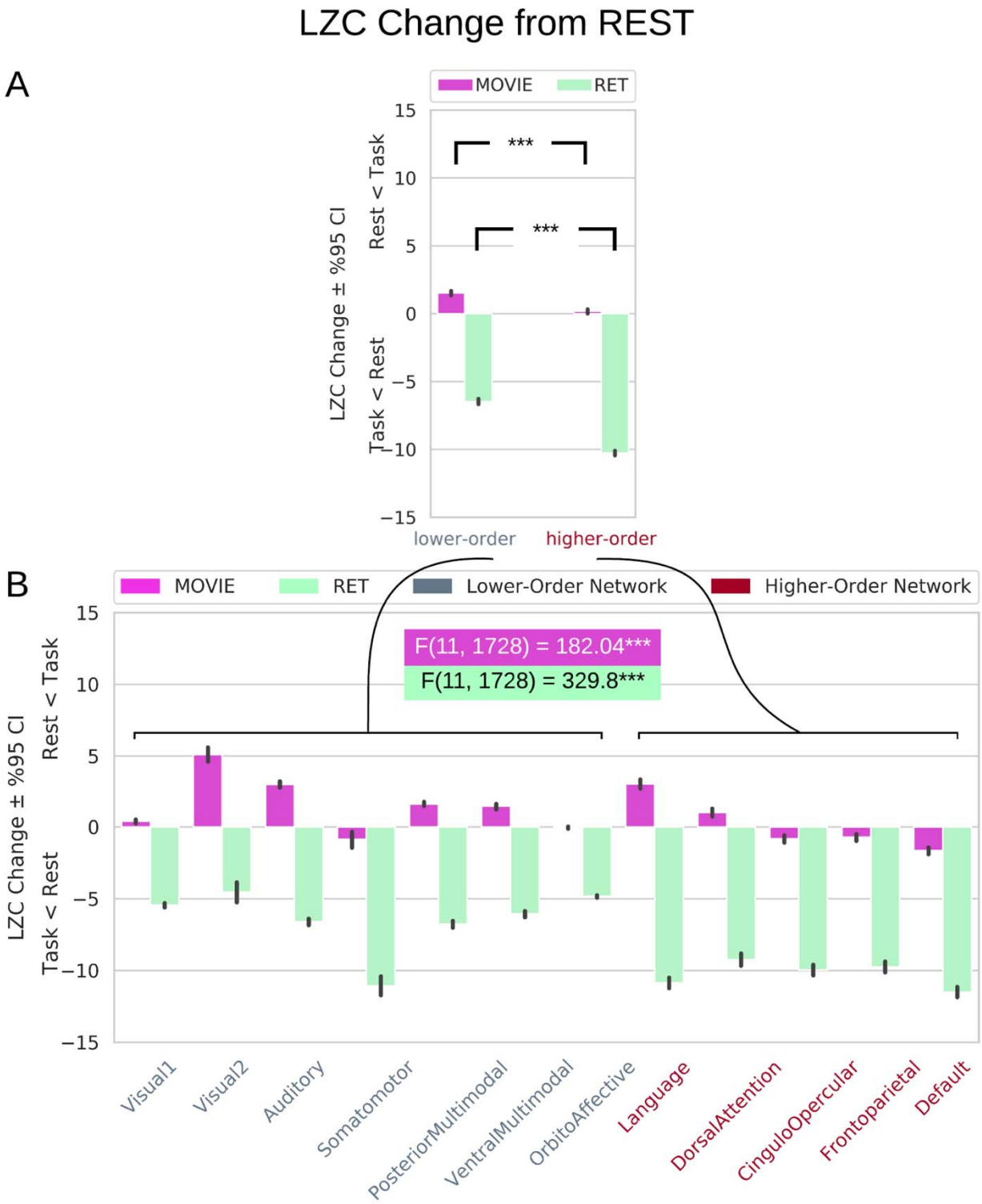

Fig. 4. Change in LZC from rest to task (LZCc). *All bars are the averaged LZC ± %95 confidence interval over subjects.* ***(A)*** *LZCc for MOVIE and RET for lower- and higher-order networks. The paired student's t-test between LON and HON was significant with T = 19.54 for MOVIE and T = 24.97 for RET at* $\alpha = 0.001$. ***(B)*** *LZCc for the two task conditions for the 12 networks. One-way ANOVA showed a significant difference among the networks with F(11, 1728) = 182.04 for MOVIE and F(11, 1728) = 329.8 for RET at* $\alpha = 0.001$.

Temporal dynamics - Median Frequency in rest and task states

In order to link the LZC in rest and task states to a direct measurement of the frequencies themselves, we indexed the distribution of the power spectral density (PSD) using the Median frequency (MF). MF was chosen to provide a summary measure of the distribution of low versus high frequencies in the PSD (Fig. 5A, see also Methods for the details). Calculating MF over different brain networks revealed a topographical distribution analogous to the one of LZC, that is, higher MF in LON and lower MF in HON networks (Fig. 5B) in general and all 12 networks (Fig. 5C; see supplementary results for details; these results were also replicated in 3T dataset in Supp. Fig. 8). Next, we calculated the regional correlations (a correlation per region across regions, check Methods for details) between the two measurements in each condition (Fig. 6A). This revealed a variety of correlation values for the LZC-MF relationship across the wide range of 0.43 to 0.88 across the different regions. Given such a wide range of correlation values, we assumed that topographical differences strongly shape LZC-MF relationship; this was addressed in subsequent analyses.

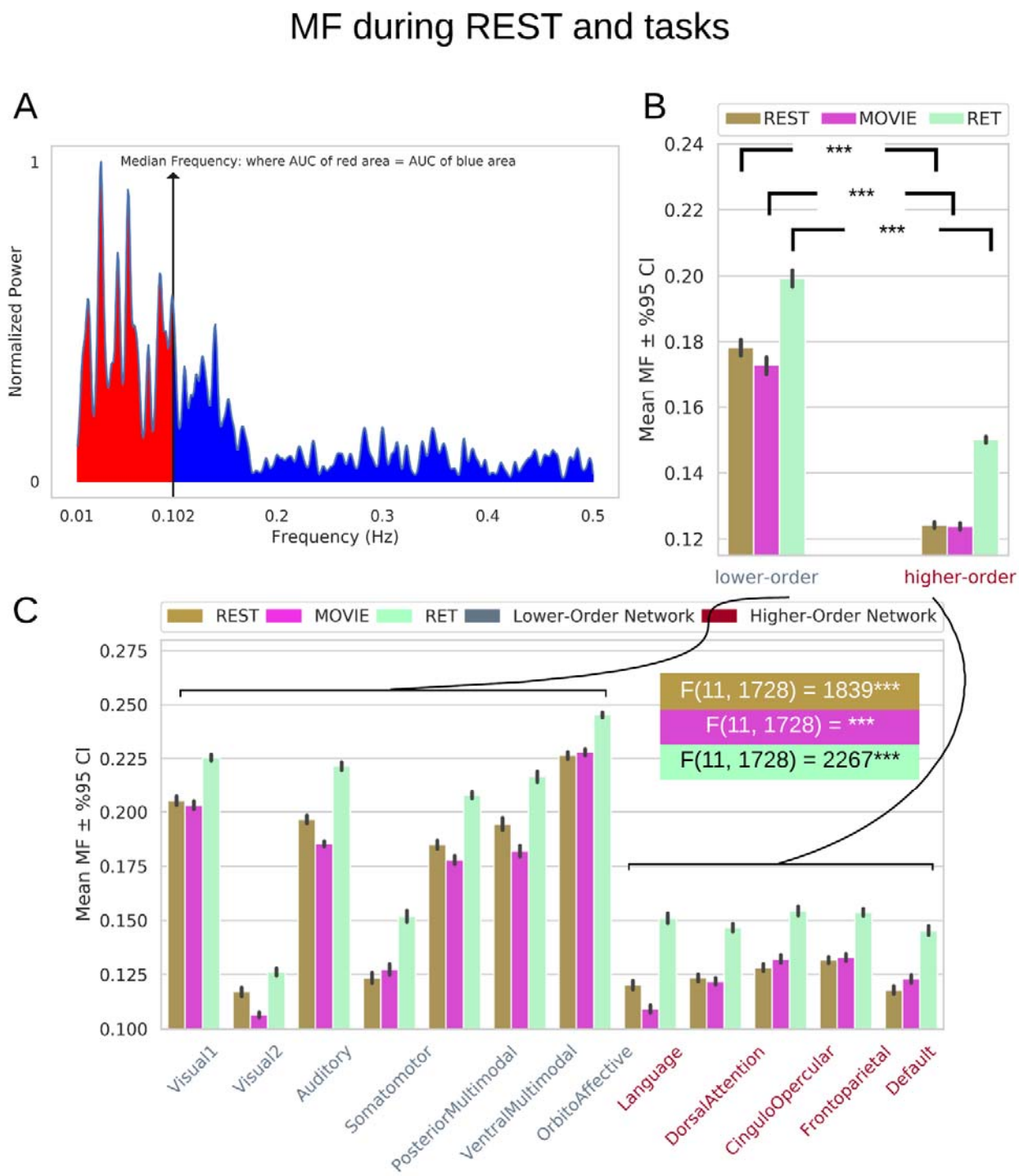

Fig. 5. MF during both rest and task states. *All bars are the averaged MF ± %95 confidence interval over subjects.* ***(A)*** *A power spectrum of a sample signal. Median frequency is calculated as the frequency at which the area under the curve (AUC) of power up to that frequency (red area) is equal to AUC beyond that point (blue area).* ***(B)*** *MF for the three conditions for lower- and higher-order networks. The paired student's t-test between LON and HON is significant with T = 77.54 for REST, T = 100.0 for MOVIE and T = 85.28 for RET at* $\alpha = 0.001$. ***(C)*** *MF over the 12 networks. One-way ANOVA showed a significant difference among the networks with F(11, 1728) = 1839 for REST, F(11, 1728) = 2400 for MOVIE and RET: F(11, 1728) = 2267 for RET at* $\alpha = 0.001$.

The relationship between LZC and MF in rest and task states

The relationship between the two metrics was explored by looking at their values in different brain regions. First, each region's LZC value was plotted against its MF value (Fig. 6B) which suggested a non-linear

regime between LZC and MF over brain regions across all three conditions. Specifically, we observed that regions with lower MF in rest exhibited largely different LZC values in rest and task whereas regions with higher MF in rest no longer showed marked LZC differences in both rest and task. Together, this amounts to a non-linear relationship in the topography of LZC and MF with high and low MF exerting different impacts on LZC (also replicated in 3T dataset in Supp. Fig. 9).

We tested whether this non-linear relationship is specifically related to the topographical distribution of LZC and MF (topographical relationship) rather than inter-individual differences between subjects. To do so, LZC and MF values were averaged over all regions leaving a pair of MF and LZC values per subject (subject-based relationship). This (Fig. 6C) revealed a linear relationship for MF-LZC relationship based on inter-individual differences. This suggests that the trend of the subject-based relationship seems linear but it is something that we cannot be sure of because it has a smaller range of values compared to the topographical relationship. In light of this non-linear relationship, we also conducted regional correlation using Spearman method between LZC and MF for each condition (Supp. Fig. 3A) to accompany our results in Fig. 6A.

This relationship was further explored by using brain's T_1w/T_2w values (see Methods) to test whether it is structurally based. T_1w/T_2w is suggested to provide a non-invasive proxy of anatomical hierarchy in primate cortex [63]. For both LZC and MF, each region's values were averaged over subjects and then the regional distribution was plotted as functions of T_1w/T_2w values (Supp. Fig. 3B top for LZC and bottom for MF). We did obtain linear relationship of LZC and MF alone with T_1w/T_2w values which contrasted with the non-linear relationship of MF and LZC we obtained in our fMRI data. That suggests that the non-linear relationship of LZC and MF holds independent of their underlying anatomical relationship; we thus assume their non-linear topographical relationship to be primarily dynamics rather than anatomical (also replicated in 3T dataset in Supp. Fig. 9).

Simulation of the relationship between LZC and MF

As a final confirmatory analysis to show the non-linearity of the LZC-MF relationship is specifically related to their topography rather than remaining independent of the latter, we decided to analyze simulated data. Seven different categories of pseudo-aleatory signals (without any topographical distribution) were simulated in the same frequency range (0.01-0.5) as our data with the same sampling rate. The categories were pink noise, white noise, sine wave, and their linear combinations (e.g. white and pink noises or white noise and sine wave). Each category contained 5000 signals (total of 35000, see Supp. Fig. 4 for a sample signal in each category).

Pink noise was utilized to simulate scale-freeness [58], sine wave for oscillation and white noise for pure randomness. The linear combination used random weights chosen from uniform distributions to bound the signals in the predefined frequency range of our real data. Calculating LZC and MF on these signals and plotting them against each other (Fig. 6D) showed no specific relationship between the two measurements. These results, thus, suggest that the non-linear relationship between MF and LZC is related to the topographical distribution of low and high MF values in different brain regions rather than remaining independent of such topographical distribution. Moreover, our simulation shows that LZC is not measuring noise in the brain thus supporting the validity of the measurement in fMRI.

The relationship between LZC rest-task change and MF-REST: the dynamic range of LZC

Is the change of LZC from rest to task in specific regions dependent upon the power spectral density, i.e., MF, of that particular region? We therefore investigated how the degree of change in LZC from rest to task

(LZCc) is related to the power spectrum during rest (MF-REST). The LZCc values of all regions were plotted against their corresponding MF values during rest (MF-REST) for both task conditions (Fig. 6E). Careful consideration of these plots alongside a mediation analysis of LZC with MF as mediator (see supplementary results for details) suggested that there might be a relationship between the range of LZCc values and MF-REST.

Following that, we decided to conduct a median-split of the MF-REST values across brain regions. That served the purpose of calculating LZCc values in dependence on low MF-REST and high MF-REST (Supp. Fig. 5). Plotting both categories with box plots (Fig. 6F), revealed a large difference in the range of LZCc values between low and high MF-REST categories. To test whether this difference is significant or not, LZCc values of each subject were divided into two categories of low and high MF-REST. Then, the significant difference between the two was confirmed by Student's t-test over subjects (MOVIE: $T = 33.48$, RET: $T = 46.00$, $p < 0.001$).

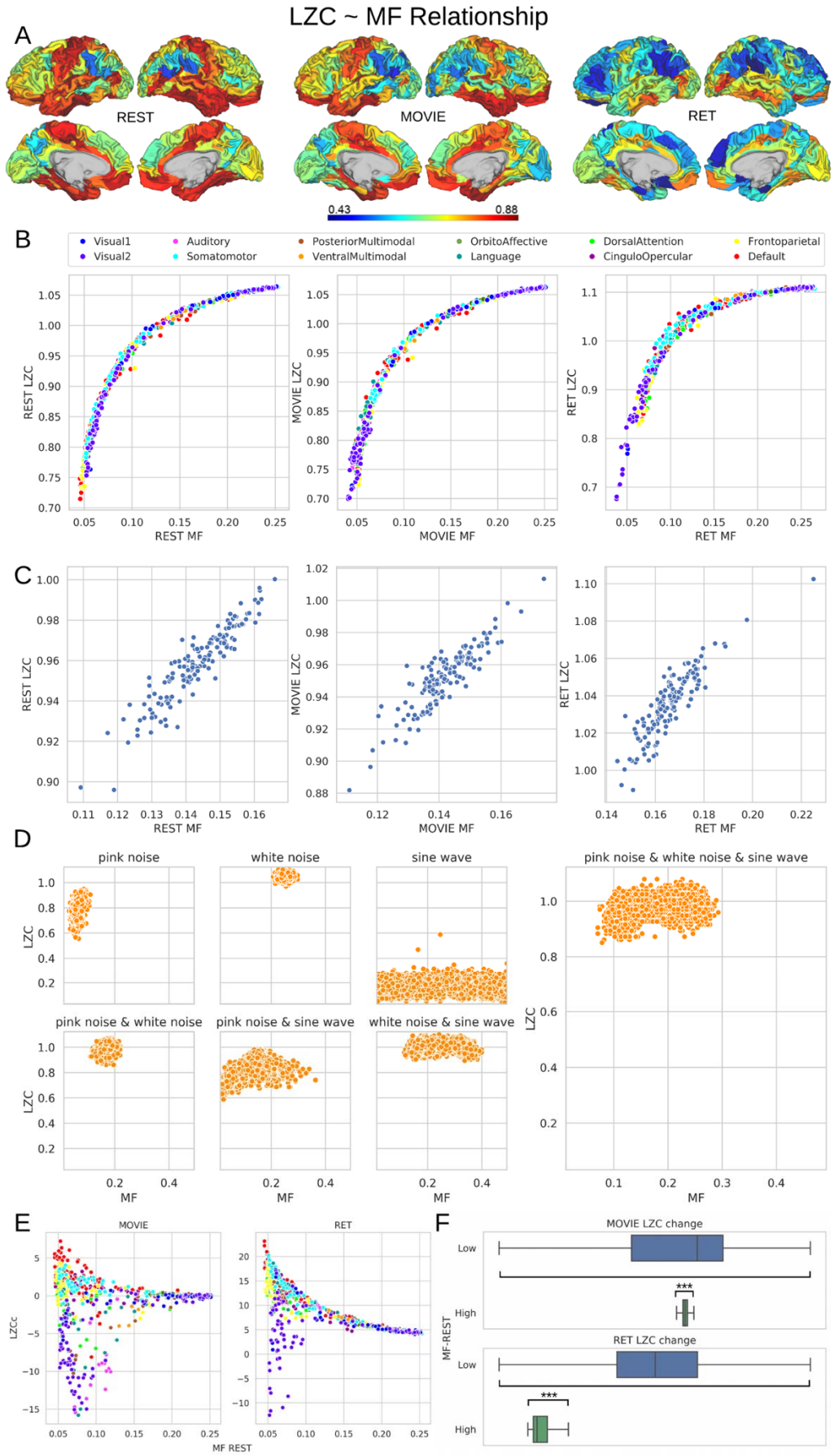

Fig. 6. The relationship between LZC and MF. (A) *Regional correlation between LZC and MF for the three conditions of REST, MOVIE and RET. Range of Pearson correlation coefficient was 0.43 to 0.88 (see supplementary*

figures for Spearman correlation). ***(B)*** *Regional scatter plots of LZC-MF relationship for the three conditions. Each point is a region averaged over subjects, and the colors show the regions belonging to specific networks. All plots show LZC as a nonlinear function of MF.* ***(C)*** *Scatter plots of LZC-MF relationship for different subjects in the three conditions. Each point is a subject averaged over regions. The nonlinear relationship can no longer be observed.* ***(D)*** *Simulation of the LZC-MF relationship with seven different types of signal. Each plot shows the distribution of LZC as a function of MF for 5000 simulated signals.* ***(E)*** *The relationship between LZCc and MF-REST. LZCc stands for the change in LZC from resting state to task state. The scatter plot of MF-REST (x-axis) vs. LZCc (y-axis) for MOVIE (left) and RET (right) conditions. The plots indicate a decrease in the range of LZCc as a function of MF-REST.* ***(F)*** *Box plots showing the range of LZCc values for low-MF and high-MF. Statistics was conducted using Student's T-Test over subjects. For each subject a range of LZCc was calculated in low and high MF categories. For both conditions (MOVIE and RET) the range of LZCc in low-MF is significantly wider than high-MF.*

These data suggest, that the range of LZCc values in low MF-REST regions is significantly higher than in high MF-REST regions which is also true for LON and HON, respectively (Supp. Fig. 6A). Together these results suggest that the range in which the region's LZC can change is associated to the level of MF-REST (low or high). Therefore, we speak of a dynamic range of LZC (drLZC) which we hypothesize to be related to PSD of the region as indexed by MF.

To further test the drLZC effect we incorporated a moderation model to see if MF-REST being low or high can moderate the relation between LZC during rest and task states. A binary moderator variable (Z) for MF-REST being low (Z = 0) or high (Z = 1) was defined. Then, the effect of LZC-REST and Z was explored on LZC during the two task conditions using linear regression (see Methods for details). The model showed significant moderation of LZC rest-task relationship with MF-REST being low or high. For MOVIE the effect of moderator was 0.08 ($T = 9.63$, $p < 0.001$). Likewise, for RET the effect of moderator was 0.42 ($T = 44.52$, $p < 0.001$). In other words, our moderation analysis suggests that the effect of LZC during REST on LZC during MOVIE (RET) can be moderated by MF during REST.

Replication with 3T data

Topographical resting state LZC/MF of 3T data. 3T resting state data was analyzed using the exact same procedure as our 7T data (Supp. Fig. 7 for LZC and 8 for MF). Difference between LON and HON was statistically tested with Paired student's t-test between across subjects which showed that both LZC and MF is significantly higher ($T = 51.05$ and $T = 132.7$, respectively, $p < 0.001$) in LON compared to HON. Furthermore, LZC and MF were also significantly different among the 12 networks tested with one-way ANOVA ($F(11, 13140) = 6348$ and $F(11, 13140) = 16571$, respectively, $p < 0.001$). These results validate our original topographical findings.

Relation between LZC and MF in 3T data. As another confirmatory analysis, the relationship between LZC and MF was investigated in resting state 3T data. Life before, first the two measurements were correlated with each other using both Pearson and Spearman methods (Supp. Fig. 9A). Moreover, LZC was plotted as a function of MF both for each region (Supp. Fig. 9B top left) and for each subject (Supp. Fig. 9A top right). The non-linear relationship over the brain regions was again observed in the 3T data. Both regional (averaged over subjects) LZC and MF were separately plotted as functions of $\sqrt{T_1w/T_2w}$ values which didn't show any specific non-linear relationship. Taken together, these results replicated our findings on LZC and MF relationship.

Discussion

We investigated the convergence of spatial and temporal topographies by using novel measures like complexity (LZC) and temporal dynamics (MF). Our main findings in both main (7T HCP) and replication (3T HCP) data sets are: (I) significantly different resting state LZC and MF in lower- and higher-order networks with the latter showing lower values in both LZC and MF; (II) task-specific LZC and MF increases and task-unspecific LZC and MF decreases during different tasks in lower- and higher-order networks; (III) non-linear topographical relationship of LZC and MF with regions showing lower rest-MF values being related to lower resting state LZC and larger capacity for rest-task LZC changes. Together, we demonstrate convergence of the brain's spatial topographical hierarchy in terms of its complexity with the temporal hierarchy of brain dynamics. This provides evidence for direct convergence of spatial and temporal dimensions in the brain's cortical topographical hierarchies which shapes both its rest and task states.

Topographical hierarchy of complexity (LZC)

We show different degrees of LZC in different networks during resting state. Higher-order networks like the DMN, FPN, language, and dorsal attention networks exhibit lower values of LZC and MF in the resting state's infraslow frequencies (ISF, $f < 0.1$). In contrast, lower-order networks like sensory networks, orbitoaffective, and multimodal networks show high LZC values. Hence, taken together, the signal and thus the neural activity is more regular and more compressible, i.e., lower LZC and then lower MF, in higher-order networks than in lower-order networks.

Our findings complement previous results that show analogous differences between lower- and higher-order networks. Spatially, lower-order networks are more locally connected while higher-order networks are more globally connected throughout the whole brain. This led recently to the so-called core-periphery organization [1,2]: lower-order unimodal networks like sensory networks are at the periphery while higher-order heteromodal networks like DMN and FPN constitute the core as they are connected throughout the whole brain. Recent data suggest such core-periphery organisation to be mirrored also in the brain's temporal organisation as its intrinsic neural timescales are shorter in the lower-order networks, i.e., the periphery, and longer in the higher-order networks, i.e., the core [10,12,14,32,33,64].). Our data strongly support such complementary temporal characterization of spatial topography.

The differential role of lower- and higher-order regions is further supported by our results in task states. We observed network- and task-specific changes during the two tasks relative to the resting state. Task-specific increases were observed for example in visual and auditory networks during movie as well as visual cortex's sub-regions during retinotopy. Together, extending findings by [38], the here observed rest-task differences in LZC further support the assumption of task- and network-specific changes in LZC and, more generally, the involvement of ISF in modulating complexity in both rest and task states.

Together, the present findings extend the differentiation of lower- and higher-order networks beyond mere spatial and temporal features to their role in complexity and brain dynamics, i.e., LZC and MF. Lower-order networks like sensory networks show more irregular and complex signal dynamics resulting in higher LZC and MF. Given that sensory networks are continuously exposed to the processing of highly irregular and complex external stimuli [32,33], their intrinsic spontaneous resting state dynamics may by itself be rather irregular and complex resulting in high LZC and MF. In contrast, higher-order networks like DMN and FPN are not exposed to direct external stimulus input such that their intrinsic ongoing dynamics is not as much constrained by the irregular external stimulus input [32,33,65] – their signal dynamics may thus be more regular and less complex resulting in lower resting state LZC and MF values as observed and replicated in our data.

Brain dynamics (MF) drive spatial topography (LZC)

In order to test whether the regions' LZC is related to their temporal dynamics, we additionally investigated the power spectral density of ISF measured by MF. MF showed a topographical pattern more or less similar to the one as LZC with low MF in higher-order and high MF in lower-order networks during both rest and task. This suggests a close relationship of LZC to MF. Spatial correlation confirmed such a close relationship; however, regional MF-LZC correlation revealed quite a variety of different degrees in their correlation within the different regions. Such wide variety of LZC-MF correlation across different regions suggests differential relationship of regions with low and high MF to LZC. This was confirmed in various lines of subsequent analyses.

We obtained a non-linear topographical pattern in the LZC-MF relationship in both rest and task states. Regions with low MF at rest showed lower rest LZC and more differentiation in their respective LZC rest-task changes than those regions exhibiting high rest MF. We could further demonstrate that such non-linear relationship was related specifically to the topographical distribution of low and high MF values rather than being associated with inter-individual differences, anatomical differences in T1/T2 of the different regions, or some LZC-MF relationship independent of their topographical distribution (as tested for in simulation).

Further, we observed that the MF impacted the range of possible LZC rest-task changes. Regions with low MF values showed much larger changes in their rest-task LZC values than those with high MF (see supplementary results). Hence, MF in rest seems to modulate the capacity for change in LZC during the transition from rest to task: regions with low MF and thus more power in the slower ISF ranges have a higher likelihood of exhibiting larger changes, i.e., increases or decreases, during the transition from rest to task states. While this was somewhat related to lower- and higher-order network regions, the main driving factor is the region's degree of MF, that is, whether it is low or high. Hence, it is the brain dynamics of the different regions rather than the regions themselves (independent of their dynamics) that drives topographical distribution of LZC during rest and task.

Low values in MF reflect stronger power in the very infraslow frequency fluctuations which can be characterized by extremely long cycle durations. These long cycle durations are assumed to be ideal for summing and pooling different stimuli occurring at different points in time such that their respective information is processed and thus lumped together [24,27,30,57,65]. Such summing and pooling may enable higher degrees of integration of temporally distinct stimuli. That, in turn, leads to a more regular and therefore less complex signal dynamics with lower LZC values. One would consequently expect that regions showing lower values in MF should also exhibit lower LZC values which is exactly what we observed in our data.

This supposed modulation of LZC-MF relationship by the pooling and summing of stimuli through cycle duration may also account for the observed differences in the rest-task changes of the LZC in regions with low and high MF. If a region shows low MF, the power of its long cycle duration is stronger than the one of a region with higher MF. That may allow the low rest MF region to pool, sum, and ultimately integrate more external stimuli during task states [57] than a region with high rest MF. This, in turn, changes the degree of that region's complexity and thus its LZC to a large degree. This stands in contrast to a high rest MF region that, due to its lower power in the long cycle duration, cannot pool and sum as many external stimuli and consequently cannot much change its LZC from rest to task. That remains to be tested in future modelling studies though.

Limitations

There are a few considerations which should be considered in this study. First, task-unspecificity should also be replicated using different tasks in different modalities and domains; however, with respect to our metrics, we included two tasks with completely different complexity and temporal structure. The movie presents a

continuous task while the retinopathy is a clearly event-related trial-based discontinuous task - the inclusion of tasks with two different task structures accounts for the recent suggestion of considering and including task with different structures, i.e., continuous and trial-based [66]. Second, this study contains no behavioral measurement, but on the other hand, the tasks measured pure perception and stimulus processing with no interference of cognitive demands, thus no-report paradigms as distinguished from report paradigms [67]. The reliance on no-report paradigms allowed to isolate clearly stimulus-related effects, i.e., movie and visual stimuli during retinopathy, as they are supposed to be related to, specifically, primary sensory networks like visual and auditory networks. Hence, the no-report paradigms are ideal to test the response of primary networks independent of any task-related confounds as in report paradigms.

Conclusion

We demonstrate the convergence of spatial and temporal hierarchies in the brain and how that shapes rest and task states. Our key finding is that the spatial hierarchy in the complexity of lower- and higher-order networks converges with their temporal dynamics. Even more important, we show that the temporal dynamics, that is, the degree of power in the different regions' infraslow frequencies, strongly shapes the topographical distribution of their complexity during rest and task states in a non-linear way. In conclusion, we unravel the intimate connection of spatial and temporal dimensions in cortical hierarchies including their shaping by the brain's intrinsic dynamics. This contributes to better understand the complex topographical activation pattern during perception and cognition as well as their changes in psychiatric disorders like schizophrenia and depression.

Acknowledgments

This research has received funding from the European Union's Horizon 2020 Framework Program for Research and Innovation under the Specific Grant Agreement No. 785907 (Human Brain Project SGA2). GN is grateful for funding provided by UMRF, uOBMRI, CIHR and PSI.

Materials and Methods

Experimental Design

Data was selected from Human Connectome Project's 7T dataset (rather than HCP 3T) in order to achieve a high signal to noise ratio (SNR) (and to have more fine-grained resolution) which is especially relevant for properly capturing temporospatial dynamics. Other reasons for choosing the 7T data were the longer and more continuous scanning during task states. We used HCP 3T resting-state data for validation purposes; in contrast, we did not use the task data of 3T dataset because of their short block design which makes proper measurement of the dynamics with our measures impossible.

From the data of 1200 subjects released in HCP-1200 [68], 146 of them had completed the full 7T imaging protocol of human connectome project (HCP) without any imaging quality issues. A total of 14 fMRI runs (TR=1s) including four resting-state (REST), four movie-watching (MOVIE), and six retinotopy (RET) of these participants were used in this study. Full details on data acquisition and preprocessing are provided in separate articles [69,70]. In each MOVIE run, subjects had to watch a movie of approximately 15 minutes consisting of several clips separated by 20-seconds rest periods. Different clips were used in different runs (Details are available at HCP S1200 Release Reference). For RET, stimuli were constructed by creating slowly moving apertures and placing a dynamic colorful texture within the apertures [Check [71] for details].

Preprocessed data was downloaded from HCP database at https://db.humanconnectome.org. The preprocessing pipeline includes registration to MNI space, alignment for motion, fieldmap correction, FIX denoising, and MSMAll group registration. Full details of all the steps are available in [69,72].

Data Processing & Statistical Analysis

All steps of the data processing were performed with in-house scripts written in Python programming language using numpy, scipy, cifti, joblib, matplotlib, and seaborn libraries. The source code is freely available at www.georgnorthoff.com/codes/. For brain map visualization purposes, wb_view (part of Connectome Workbench software, https://www.humanconnectome.org/software/connectome-workbench) was used.

All statistical analyses were performed in the statsmodel library [73] in Python and R v.3.6 and all p-values were corrected for multiple comparison using the bonferroni method at $\alpha = 0.001$. The student's t-test was used to measure the statistical differences between LON and HON networks. Moreover, one-way ANOVA with twelve factors for the 12 networks was used to investigate the difference between the networks during each condition.

Template and network definition. The preprocessed data were high-pass filtered at 0.01 in order to both maintain the full frequency spectrum of the data [74] and remove noise. After that, signals were averaged over brain regions defined in the template provided by [60] to get one fMRI signal per region per subject per run (Fig. 1A). The template contains 717 regions categorized into 12 networks of visual1, visual2, auditory, somatomor, posterior multimodal, ventral multimodal, orbitoaffective, language, dorsal attention, cingulopercular, frontoparietal, and default-mode. To investigate our lower-order vs. higher-order hypothesis, we also divided the regions into lower-order (LON) and higher-order (HON) networks. LON included the regions in the visual1, visual2, auditory, somatomotor, posterior multimodal, ventral multimodal and orbitoaffective networks. Regions inside language, dorsal attention, cingulopercular, frontoparietal, and default-mode networks were put under the HON category. For replication purposes, another more conservative division (LIH division) was also used in which the regions in visual, auditory, and somatomotor

networks were put in the lower-order category and the regions in cingulo opercular, frontoparietal, and default-mode were put in higher-order category.

LZC calculation. In order to calculate the Lempel-Ziv complexity (LZC), first, the signal was converted into a binary sequence. Previous studies [35,75] suggest that the median of the signal's amplitude is a good candidate to use as a binarization threshold. After binarizing each region's signal and converting it to a string sequence, the LZC algorithm [34] was used to compute. As earlier studies have pointed out, LZC is dependent on the length of the sequence, thus a normalization factor (more info in [35]) was used to remove that effect. LZC processing is illustrated in Fig. 1A.

MF calculation. Median frequency (MF) was measured by first calculating power spectral density (PSD) of each region's signal. PSD was calculated using the Welch algorithm [76] with hanning window implemented in the Scipy package of Python programming language. The median frequency (MF) was calculated from the PSD as the frequency which divides the area under the curve into two halves (Fig. 5A).

Rest and task topographical calculations. The values of both measurements were first calculated for each of the 14 fMRI runs and then averaged over the four runs in all three conditions (REST, MOVIE and RET). After that, based on the requirements of each analysis the values were either averaged over the LON-HON division or the 12 aforementioned networks. LON was compared to HON using Student's T-Test over subjects. Also, statistical comparison among the networks were performed by one-way ANOVA with 12 levels for the 12 networks.

Spatial correlation. To calculate the spatial similarity between different conditions, spatial correlation was performed. For a pair conditions (e.g. REST and MOVIE), first, a single brain for each one was calculated by averaging the values (e.g. LZC) across subjects, then a single Pearson correlation coefficient was calculated over the regions.

Regional correlation. To calculate similarity between two topographical maps, regional correlation was conducted. For each region a single Pearson (or Spearman, depending on the analysis) correlation coefficient was calculated over subjects between a pair of maps (e.g. LZC during REST and MF during REST). Then, these coefficients were mapped on to the brain template.

Percentage of change from rest. The difference between rest and task state was calculated as a percentage of change per region per subject. Each region's REST and task (e.g. MOVIE) values was put in the $\frac{TASK - REST}{REST} \times 100$ formula to both measure the change from rest to task and normalize against rest at the same time. Then, for each subject the percentage change values were either averaged over the 12 networks or along the LON-HON division. The difference between LON and HON and the difference among the networks were statistically tested using the Student's T-Test and one-way ANOVA methods, respectively.

Visual cortex. To map the visual cortex, a template by [62] was used. The fMRI signals were averaged over the visual regions provided by this template and the rest of the brain was ignored. Then, LZC and MF analyzes were performed similarly to before.

T_1w/T_2w ***map.*** The ratio between T1- to T2-weighted images is suggested to provide a non-invasive neuroimaging proxy of anatomical hierarchy in primate cortex [63]. So, we used it to investigate whether the relationship between LZC and MF is anatomically based. A cortical map containing the T_1w/T_2w was provided with the HCP dataset. The map was MSMAll registered and bias field-corrected. We parcellated the map into the regions/networks of our template by averaging the T_1w/T_2w values inside each region.

LZC-MF simulation. The relationship between LZC and MF was explored using simulated signals. 35000 pseudo-aleatory signals within seven different categories (5000 each, see Supp. Fig. 4 for a sample signal in each category) were simulated to investigate whether the LZC-MF relationship is non-linear or not and whether the relationship is specific to the brain. The seven categories were (I) pink noise, (II) white noise, (III) sine wave, and linear combinations of (IV) pink and white noises (V) pink noise and sine wave (VI) white noise and sine wave and (VII) pink noise, white noise and sine wave.

Random weights were chosen for the linear combinations and also the sine wave used different random frequencies. All random values were chosen from a uniform distribution and were controlled to produce signals in the same frequency range of our original data (0.01-0.5 Hz). Pink noise was chose to model the scale-free behavior [58], white noise for pure randomness and sine wave for oscillation. The MF and LZC were calculated for each signal and used to further investigate the relationship between the two measurements, and validate LZC calculations in fMRI data.

LZCc-MF-REST mediation model. In order to investigate the effect of MF during rest (MF-REST) on LZC change from rest to task (LZCc), a mediation model was performed using the mediation library in R. Two separate models were created for the two task conditions. Each model consisted of MF-REST as the mediator, LZC during REST as the independent variable (IV) and LZC during the task as the dependent variable (DV). After running the model and observing indirect effects of IV on DV, the significance of that effect was tested using bootstrapping procedures [77,78]. Unstandardized indirect effects were computed for each of 1000 bootstrapped samples, and the 95% confidence interval was computed by determining the indirect effects at the 2.5th and 97.5th percentiles.

LZCc-MF-REST moderation model. To further investigate the relationship between LZCc and MF-REST, regions were divided into two categories based on their MF-REST values. The median of MF-REST was used as the threshold and the regions with lower (higher) MF-REST than the median was put into the low (high) MF-REST category. The median was used to balance the two categories. A new binary variable (Z) was created for each region's MF-REST category (0 = low MF-REST and 1 = high MF-REST). Z was injected in a linear regression model as a moderator: $Y = \beta_1 X + \beta_2 Z + \beta_3 XZ + \beta_4$. In the linear regression equation, Y is LZC during task state, X is LZC during resting state, and Z is the binary value of MF during resting state.

References

1. Margulies, D. S. *et al.* Situating the default-mode network along a principal gradient of macroscale cortical organization. *Proc. Natl. Acad. Sci. U. S. A.* **113**, 12574–12579 (2016).
2. Huntenburg, J. M., Bazin, P. L. & Margulies, D. S. Large-Scale Gradients in Human Cortical Organization. *Trends Cogn. Sci.* **22**, 21–31 (2018).
3. Wang, P. *et al.* Inversion of a large-scale circuit model reveals a cortical hierarchy in the dynamic resting human brain. *Trop. Subtrop. Agroecosystems* **21**, (2019).
4. Murphy, C. *et al.* Distant from input: Evidence of regions within the default mode network supporting perceptually-decoupled and conceptually-guided cognition. *Neuroimage* **171**, 393–401 (2018).
5. Cole, M. W., Bassett, D. S., Power, J. D., Braver, T. S. & Petersen, S. E. Intrinsic and task-evoked network architectures of the human brain. *Neuron* (2014) doi:10.1016/j.neuron.2014.05.014.
6. Cole, M. W., Ito, T., Bassett, D. S. & Schultz, D. H. Activity flow over resting-state networks shapes cognitive task activations. *Nat. Neurosci.* (2016) doi:10.1038/nn.4406.
7. Huang, Z. *et al.* Is There a Nonadditive Interaction Between Spontaneous and Evoked Activity? Phase-Dependence and Its Relation to the Temporal Structure of Scale-Free Brain Activity. *Cereb. Cortex* **27**, 1037–1059 (2017).
8. Huang, Z., Liu, X., Mashour, G. A. & Hudetz, A. G. Timescales of intrinsic BOLD signal dynamics and functional connectivity in pharmacologic and neuropathologic states of unconsciousness. *J. Neurosci.* **38**, 2304–2317 (2018).
9. Hasson, U., Chen, J. & Honey, C. J. Hierarchical process memory: Memory as an integral component of information processing. *Trends Cogn. Sci.* **19**, 304–313 (2015).
10. Kiebel, S. J., Daunizeau, J. & Friston, K. J. A hierarchy of time-scales and the brain. *PLoS Comput. Biol.* **4**, e1000209 (2008).
11. Chaudhuri, R., He, B. J. & Wang, X. J. Random recurrent networks near criticality capture the broadband power distribution of human ECoG dynamics. *Cereb. Cortex* **28**, 3610–3622 (2018).
12. Chaudhuri, R., Knoblauch, K., Gariel, M. A., Kennedy, H. & Wang, X. J. A Large-Scale Circuit Mechanism for Hierarchical Dynamical Processing in the Primate Cortex. *Neuron* **88**, 419–431 (2015).
13. He, B. J. Scale-free properties of the functional magnetic resonance imaging signal during rest and task. *J. Neurosci.* **31**, 13786–13795 (2011).
14. Murray, R. J., Debbané, M., Fox, P. T., Bzdok, D. & Eickhoff, S. B. Functional connectivity mapping of regions associated with self- and other-processing. *Hum. Brain Mapp.* **36**, 1304–1324 (2015).
15. Chen, J. *et al.* Shared memories reveal shared structure in neural activity across individuals. *Nat. Neurosci.* **20**, 115–125 (2017).
16. Bijsterbosch, J. *et al.* Investigations into within- and between-subject resting-state amplitude variations. *Neuroimage* **159**, 57–69 (2017).
17. Chen, J., Hasson, U. & Honey, C. J. Processing Timescales as an Organizing Principle for Primate Cortex. *Neuron* (2015) doi:10.1016/j.neuron.2015.10.010.
18. Chaudhuri, R., Bernacchia, A. & Wang, X.-J. A diversity of localized timescales in network activity. *Elife* (2014) doi:10.7554/elife.01239.
19. Chaudhuri, R., Gerçek, B., Pandey, B., Peyrache, A. & Fiete, I. The intrinsic attractor manifold and population dynamics of a canonical cognitive circuit across waking and sleep. *Nat. Neurosci.* (2019) doi:10.1038/s41593-019-0460-x.
20. Huang, Z., Zhang, J., Wu, J., Mashour, G. A. & Hudetz, A. G. Temporal circuit of macroscale dynamic brain activity supports human consciousness. *Sci. Adv.* (2020) doi:10.1126/sciadv.aaz0087.
21. Stephens, G. J., Honey, C. J. & Hasson, U. A place for time: The spatiotemporal structure of neural dynamics during natural audition. *J. Neurophysiol.* (2013) doi:10.1152/jn.00268.2013.
22. Simony, E. *et al.* Dynamic reconfiguration of the default mode network during narrative comprehension. *Nat. Commun.* (2016) doi:10.1038/ncomms12141.
23. Buzsáki, G. *Rhythms of the Brain*. *Rhythms of the Brain* (2009). doi:10.1093/acprof:oso/9780195301069.001.0001.
24. He, B. J. & Raichle, M. E. The fMRI signal, slow cortical potential and consciousness. *Trends Cogn. Sci.* **13**, 302–309 (2009).
25. Steriade, M., Nunez, A. & Amzica, F. A novel slow (< 1 Hz) oscillation of neocortical neurons in vivo: Depolarizing and hyperpolarizing components. *J. Neurosci.* **13**, 3252–3265 (1993).
26. Baria, A. T., Maniscalco, B. & He, B. J. Initial-state-dependent, robust, transient neural dynamics encode conscious visual perception. *PLoS Comput. Biol.* **13**, e1005806 (2017).
27. Li, Q., Hill, Z. & He, B. J. Spatiotemporal dissociation of brain activity underlying subjective awareness, objective performance and confidence. *J. Neurosci.* (2014) doi:10.1523/JNEUROSCI.1820-13.2014.
28. Khader, P., Schicke, T., Röder, B. & Rösler, F. On the relationship between slow cortical potentials and BOLD signal changes in humans. *Int. J. Psychophysiol.* (2008) doi:10.1016/j.ijpsycho.2007.05.018.
29. Buzsáki, G. The Brain from Inside Out. *The Brain from Inside Out* (2019) doi:10.1093/oso/9780190905385.001.0001.
30. Northoff, G. “Paradox of slow frequencies” – Are slow frequencies in upper cortical layers a neural predisposition of the level/state of consciousness (NPC)? *Conscious. Cogn.* **54**, 20–35 (2017).

31. Gutierrez-Barragan, D., Basson, M. A., Panzeri, S. & Gozzi, A. Infraslow State Fluctuations Govern Spontaneous fMRI Network Dynamics. *Curr. Biol.* **29**, 2295-2306.e5 (2019).
32. Gollo, L. L. *et al.* Dwelling quietly in the rich club: Brain network determinants of slow cortical fluctuations. *Philos. Trans. R. Soc. B Biol. Sci.* **370**, 20140165 (2015).
33. Gollo, L. L., Roberts, J. A. & Cocchi, L. Mapping how local perturbations influence systems-level brain dynamics. *Neuroimage* **160**, 97–112 (2017).
34. Lempel, A. & Ziv, J. On the Complexity of Finite Sequences. *IEEE Trans. Inf. Theory* (1976) doi:10.1109/TIT.1976.1055501.
35. Aboy, M., Hornero, R., Abásolo, D. & Álvarez, D. Interpretation of the Lempel-Ziv complexity measure in the context of biomedical signal analysis. *IEEE Trans. Biomed. Eng.* **53**, 2282–2288 (2006).
36. Varley, T. F. *et al.* Consciousness & Brain Functional Complexity in Propofol Anaesthesia. *Sci. Rep.* **10**, 1018 (2020).
37. Deshpande, G., LaConte, S., Peltier, S. & Hu, X. Tissue specificity of nonlinear dynamics in baseline fMRI. *Magn. Reson. Med.* **55**, 626–632 (2006).
38. Boly, M. *et al.* Stimulus set meaningfulness and neurophysiological differentiation: A functional magnetic resonance imaging study. *PLoS One* **10**, e0125337 (2015).
39. Hudetz, A. G., Liu, X., Pillay, S., Boly, M. & Tononi, G. Propofol anesthesia reduces Lempel-Ziv complexity of spontaneous brain activity in rats. *Neurosci. Lett.* **628**, 132–135 (2016).
40. Gómez, C., Hornero, R., Abásolo, D., Fernández, A. & Escudero, J. Analysis of MEG background activity in Alzheimer's disease using nonlinear Methods and ANFIS. *Ann. Biomed. Eng.* **37**, 586–594 (2009).
41. Fernández, A. *et al.* The correlation between white-matter microstructure and the complexity of spontaneous brain activity: A difussion tensor imaging-MEG study. *Neuroimage* **57**, 1300–1307 (2011).
42. Luo, Q. *et al.* Complexity analysis of resting state magnetoencephalography activity in traumatic brain injury patients. *J. Neurotrauma* **30**, 1702–1709 (2013).
43. Baria, A. T. *et al.* Bold temporal variability differentiates wakefulness from anesthesia-induced unconsciousness. *J. Neurophysiol.* **119**, 834–848 (2018).
44. Abásolo, D., Hornero, R., Gómez, C., García, M. & López, M. Analysis of EEG background activity in Alzheimer's disease patients with Lempel-Ziv complexity and central tendency measure. *Med. Eng. Phys.* **28**, 315–322 (2006).
45. Abasólo, D., James, C. J. & Hornero, R. Non-linear analysis of intracranial electroencephalogram recordings with approximate entropy and lempel-ziv complexity for epileptic seizure detection. in *Annual International Conference of the IEEE Engineering in Medicine and Biology - Proceedings* vol. 6 1953–1956 (IEEE, 2007).
46. Bachmann, M. *et al.* Methods for classifying depression in single channel EEG using linear and nonlinear signal analysis. *Comput. Methods Programs Biomed.* **155**, 11–17 (2018).
47. Ibáñez-Molina, A. J. *et al.* EEG multiscale complexity in schizophrenia during picture naming. *Front. Physiol.* **9**, 1213 (2018).
48. Mateos, D. M., Guevara Erra, R., Wennberg, R. & Perez Velazquez, J. L. Measures of entropy and complexity in altered states of consciousness. *Cogn. Neurodyn.* **12**, 73–84 (2018).
49. Szczepański, J., Amigó, J. M., Wajnryb, E. & Sanchez-Vives, M. V. Application of Lempel-Ziv complexity to the analysis of neural discharges. *Netw. Comput. Neural Syst.* **14**, 335–350 (2003).
50. Schwilden, H., Schuttler, J. & Stoeckel, H. Quantitation of the EEG and pharmacodynamic modelling of hypnotic drugs: etomidate as an example. *Eur. J. Anaesthesiol.* **2**, 121–131 (1985).
51. Schwender, D. *et al.* Spectral edge frequency of the electroencephalogram to monitor 'depth' of anaesthesia with isoflurane or propofol. *Br. J. Anaesth.* **77**, 179–184 (1996).
52. McDonald, T., Berkowitz, R. & Hoffman, W. E. Median eeg frequency is more sensitive to increases in sympathetic activity than bispectral index. *J. Neurosurg. Anesthesiol.* **11**, 255–259 (1999).
53. Bachiller, A. *et al.* Decreased entropy modulation of EEG response to novelty and relevance in schizophrenia during a P300 task. *Eur. Arch. Psychiatry Clin. Neurosci.* **265**, 525–535 (2015).
54. Verrusio, W. *et al.* The Mozart Effect: A quantitative EEG study. *Conscious. Cogn.* **35**, 150–155 (2015).
55. Fox, M. D. *et al.* The human brain is intrinsically organized into dynamic, anticorrelated functional networks. *Proc. Natl. Acad. Sci. U. S. A.* **102**, 9673–9678 (2005).
56. Pappas, I., Adapa, R. M., Menon, D. K. & Stamatakis, E. A. Brain network disintegration during sedation is mediated by the complexity of sparsely connected regions. *Neuroimage* (2019) doi:10.1016/j.neuroimage.2018.10.078.
57. Himberger, K. D., Chien, H. Y. & Honey, C. J. Principles of Temporal Processing Across the Cortical Hierarchy. *Neuroscience* vol. 389 161–174 (2018).
58. He, B. J., Zempel, J. M., Snyder, A. Z. & Raichle, M. E. The temporal structures and functional significance of scale-free brain activity. *Neuron* **66**, 353–369 (2010).
59. He, B. J. Scale-free brain activity: Past, present, and future. *Trends in Cognitive Sciences* (2014) doi:10.1016/j.tics.2014.04.003.
60. Ji, J. L. *et al.* Mapping the human brain's cortical-subcortical functional network organization. *Neuroimage* **185**, 35–57 (2019).
61. Zhang, J. & Rowe, J. B. The neural signature of information regularity in temporally extended event sequences. *Neuroimage* (2015) doi:10.1016/j.neuroimage.2014.12.021.

62. Wang, L., Mruczek, R. E. B., Arcaro, M. J. & Kastner, S. Probabilistic maps of visual topography in human cortex. *Cereb. Cortex* (2015) doi:10.1093/cercor/bhu277.
63. Burt, J. B. *et al.* Hierarchy of transcriptomic specialization across human cortex captured by structural neuroimaging topography. *Nat. Neurosci.* (2018) doi:10.1038/s41593-018-0195-0.
64. Baldassano, C. *et al.* Discovering Event Structure in Continuous Narrative Perception and Memory. *Neuron* **95**, 709-721.e5 (2017).
65. Northoff, G. *Unlocking the Brain. Unlocking the Brain* (2014). doi:10.1093/acprof:oso/9780199826995.001.0001.
66. Huk, A., Bonnen, K. & He, B. J. Beyond trial-based paradigms: Continuous behavior, ongoing neural activity, and natural stimuli. *J. Neurosci.* **38**, 7551–7558 (2018).
67. Tagliazucchi, E., Carhart-Harris, R., Leech, R., Nutt, D. & Chialvo, D. R. Enhanced repertoire of brain dynamical states during the psychedelic experience. *Hum. Brain Mapp.* **35**, 5442–5456 (2014).
68. Van Essen, D. C. *et al.* The WU-Minn Human Connectome Project: An overview. *Neuroimage* **80**, 62–79 (2013).
69. Glasser, M. F. *et al.* The minimal preprocessing pipelines for the Human Connectome Project. *Neuroimage* **80**, 105–124 (2013).
70. Thanh Vu, A. *et al.* Tradeoffs in pushing the spatial resolution of fMRI for the 7T Human Connectome Project. *Neuroimage* **154**, 23–32 (2017).
71. Benson, N. C. *et al.* The Human Connectome Project 7 Tesla retinotopy dataset: Description and population receptive field analysis. *J. Vis.* **18**, 1–22 (2018).
72. Salimi-Khorshidi, G. *et al.* Automatic denoising of functional MRI data: Combining independent component analysis and hierarchical fusion of classifiers. *Neuroimage* **90**, 449–468 (2014).
73. Seabold, S. & Perktold, J. *Statsmodels: Econometric and Statistical Modeling with Python. PROC. OF THE 9th PYTHON IN SCIENCE CONF* (2010).
74. Craig, M. M., Manktelow, A. E., Sahakian, B. J., Menon, D. K. & Stamatakis, E. A. Spectral diversity in default mode network connectivity reflects behavioral state. *J. Cogn. Neurosci.* (2018) doi:10.1162/jocn_a_01213.
75. Nagarajan, R. Quantifying physiological data with Lempel-Ziv complexity - Certain issues. *IEEE Trans. Biomed. Eng.* **49**, 1371–1373 (2002).
76. Welch, P. D. The Use of Fast Fourier Transform for the Estimation of Power Spectra: A Method Based on Time Averaging Over Short, Modified Periodograms. *IEEE Trans. Audio Electroacoust.* **15**, 70–73 (1967).
77. Tingley, D., Yamamoto, T., Hirose, K., Keele, L. & Imai, K. Mediation: R package for causal mediation analysis. *J. Stat. Softw.* (2014) doi:10.18637/jss.v059.i05.
78. Hayes, A. F. Beyond Baron and Kenny: Statistical mediation analysis in the new millennium. *Commun. Monogr.* (2009) doi:10.1080/03637750903310360.